Available online at www.sciencedirect.com
SCIENCE DIRECT®
Journal of Solid State Chemistry 178 (2005) 3183–3189
JOURNAL OF SOLID STATE CHEMISTRY
www.elsevier.com/locate/jssc

Preparation and characterization of nanosize nickel-substituted cobalt ferrites ($Co_{1-x}Ni_xFe_2O_4$)

Sonal Singhal[a], J. Singh[a], S.K Barthwal[b], K. Chandra[a,*]

[a]*Institute Instrumentation Centre, Indian Institute of Technology, Roorkee, Roorkee-247 667, India*
[b]*Department of Physics, Indian Institute of Technology, Roorkee, Roorkee-247 667, India*

Received 4 June 2005; received in revised form 22 July 2005; accepted 23 July 2005

Abstract

Nanosize nickel-substituted cobalt ferrites were prepared using aerosol route and characterized by TEM, XRD, magnetic and Mössbauer spectroscopy. The particle size of as obtained samples was found to be ~10 nm which increases upto ~80 nm on annealing at 1200 °C. The unit cell parameter '*a*' decreases linearly with the nickel concentration due to smaller ionic radius of nickel. The saturation magnetization for all the samples after annealing at 1200 °C lies in the range 47.6–84.5 emu/g. Room temperature Mössbauer spectra of as obtained samples exhibit a broad doublet, suggesting super paramagnetic nature of the sample. The broad doublet is further resolved into two doublets corresponding to the iron atoms residing at the surface and internal regions of the particle. The samples annealed at 1200 °C showed broad sextet, which is resolved into two sextets, corresponding to tetrahedrally and octahedrally coordinated Fe cations. Cation distribution calculated using XRD and Mössbauer data indicates a decrease in Fe^{3+}(oct.)/Fe^{3+}(tet.) ratio with increasing nickel concentration.

Keywords: Nanoparticle; Saturation magnetization; Coercivity; X-ray diffraction; Mössbauer spectra; Cation distribution

1. Introduction

There is a growing interest in nanoparticles of magnetic ferrite because of their wide applications in permanent magnets, magnetic drug delivery, microwave devices and high-density information storage etc. [1,2]. Cobalt ferrite has cubic spinel structure and has been extensively studied because of its interesting magnetic properties. It has been regarded as one of the competitive candidates for high-density magnetic recording media because of its moderate saturation magnetization, high coercivity, mechanical hardness and chemical stability [3,4].

Tailhades et al. [5] studied mixed cobalt–copper spinel ferrites $Co_xCu_{1-x}Fe_2O_4$ and found that cation migration occurs during annealing. Ahn et al. [6] synthesized $CoFe_2O_4$ nanoparticles by microemulsion method and suggested that the particles behave as ferrimagnetic at 5 K but superparamagnetic at 300 K. Hanh et al. [7] synthesized cobalt ferrite powder of 4 nm size by forced hydrolysis method and reported the saturation magnetization and coercivity values of 75 emu/g and 10.3 kOe, respectively, at 5 K. Using modified oxidation process, Chinnasamy et al. [8] have synthesized cobalt ferrite particles of 15 nm size. It was reported that particles with grain size >36 nm show saturation magnetization and maximum coercivity values of 64 emu/g and 2.02 kOe, respectively. Lelis et al. [9] prepared cobalt-doped magnetites by co-precipitation method and concluded from X-ray and Mössbauer data that cobalt substitution occurs preferentially at octahedral coordination site. Chae et al. [10] prepared Al and Ti-doped $CoFe_2O_4$ by sol–gel method and found that the coercivity was smaller while saturation magnetization

*Corresponding author. Fax: +91 1332 273560.
E-mail addresses: skbarfph@iitr.ernet.in (S.K. Barthwal), chandfuc@iitr.ernet.in (K. Chandra).

0022-4596/$ - see front matter © 2005 Elsevier Inc. All rights reserved.
doi:10.1016/j.jssc.2005.07.020

was greater in $Al_{0.2}CoFe_{1.8}O_4$ (870 Oe and 72.1 emu/g), as compared to $Ti_{0.2}Co_{1.2}Fe_{1.6}O_4$ (1.56 kOe and 62.6 emu/g).

Nanosize ferrites have been prepared by various methods such as sol–gel, modified oxidation process, hydrothermal process, forced hydrolysis method, ball milling and microemulsion method, etc. [5–10]. The present work deals with the synthesis of nanoparticles of nickel-substituted cobalt ferrite ($Co_{1-x}Ni_xFe_2O_4$ where $x = 0$, 0.2, 0.4, 0.6, 0.8 and 1.0) via aerosol route. Aerosol method has the potential of producing multicomponent materials. Each aerosol contains the precursor in the exact stoichiometry as desired in the product. Particle size, degree of agglomeration, chemical homogeneity can be controlled with relative ease. Furthermore, production of powder and film by this method is commercially favourable [11–13].

The samples so prepared were characterized using transmission electron microscopy (TEM), X-ray Diffractometry (XRD), magnetic measurements and Mössbauer spectroscopy.

2. Experimental

Nanoparticles of nickel-substituted cobalt ferrites were prepared via aerosol route using a set-up described in our earlier paper [14]. The desired proportions of cobalt, nickel and iron nitrates were dissolved in water to prepare 5×10^{-2} M solutions. Air pressure, sample uptake and furnace temperature were maintained at 40 psi, 3–4 mL/min and ~650 °C, respectively, during preparation. The ferrite powder was deposited on the PTFE-coated substrate.

Elemental analysis was carried out on an electron probe microanalyzer (EPMA) (JEOL, 8600 M) and atomic absorption spectrophotometer (AAS) (GBC, Avanta), while the particle morphology was examined by TEM (Philips, EM400). The X-ray diffraction (XRD) studies were carried on X-ray diffractometer (Bruker AXS, D8 Advance) with Fe$K\alpha$ radiation and magnetic measurements were made on a vibrating sample magnetometer (VSM) (155, PAR). Mössbauer spectra were recorded on a constant acceleration transducer-driven Mössbauer spectrometer using ^{57}Co(Rh) source of 10 mCi initial activity. The spectrometer was calibrated using a natural iron foil as well as recrystallized sodium nitroprusside dihydrate (SNP) as standards.

3. Results and discussion

Results of elemental analysis for Co, Ni and Fe in all the samples carried out by EPMA and AAS were consistent within 2%. Column one of Table 1 shows the chemical formula obtained using this data.

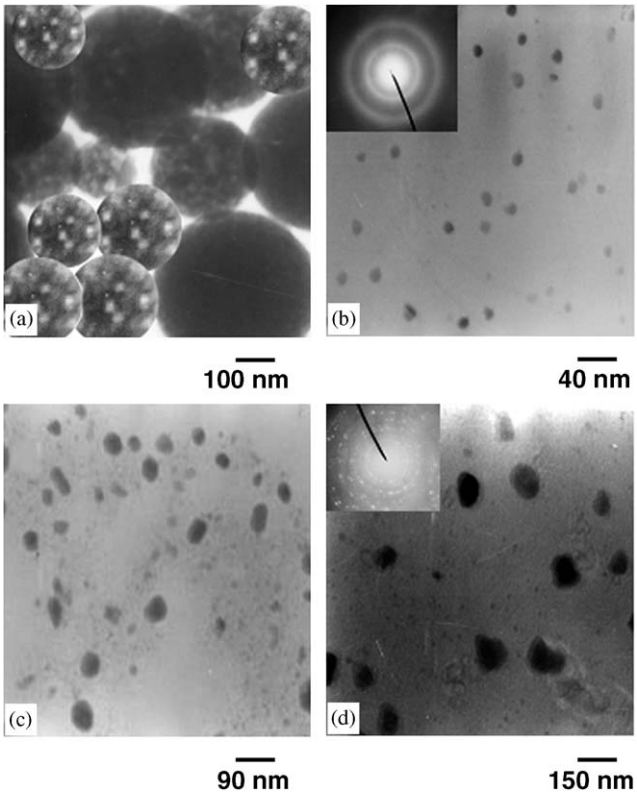

Fig. 1. Transmission electron micrographs for $Co_{0.6}Ni_{0.4}Fe_2O_4$ (a) as obtained, (b) after agitating ultrasonically, (c) after annealing at 600 °C and (d) after annealing at 1200 °C.

Table 1
Lattice parameters calculated from XRD data and saturation magnetization of the samples annealed at 1200 °C

Ferrites composition	Particle size (nm)	Lattice parameter a (Å)	Volume (Å^3)	X-ray density (g/cm^3)	Saturation magnetization (emu/g)
$CoFe_2O_4$	77.8	8.3834	589.19	5.29	84.5
$Co_{0.8}Ni_{0.2}Fe_2O_4$	77.2	8.3723	586.89	5.31	74.7
$Co_{0.6}Ni_{0.4}Fe_2O_4$	76.5	8.3682	586.00	5.32	69.3
$Co_{0.4}Ni_{0.6}Fe_2O_4$	76.1	8.3566	583.57	5.34	61.5
$Co_{0.2}Ni_{0.8}Fe_2O_4$	75.7	8.3448	581.09	5.36	53.9
$NiFe_2O_4$	75.4	8.3365	579.36	5.38	47.6

3.1. Transmission electron microscopy

The TEM micrograph of a very small amount of as obtained sample of $Co_{0.6}Ni_{0.4}Fe_2O_4$ placed on the carbon grid is shown in Fig. 1(a). Spherical particles of ~100–300 nm size can be clearly seen in the micrograph. These spherical particles consist of a large numbers of small particles held together by interfacial forces which are responsible for the spherical shape of larger (agglomerate) particles. The smaller particles could be seen inside some of the spherical particles in Fig. 1(a). Appearance of such agglomerates (large spherical particles) has also been reported in the literature [14,15]. To separate out these particles, small amount of sample was agitated ultrasonically in petroleum ether; the particles under suspension were taken on the carbon grid and dried. Micrograph of such particles (Fig. 1(b)) shows well separated particles of size ~10 nm. Selected area electron diffraction pattern (SAED) of the particle shown in the inset of Fig. 1(b) suggests the amorphous nature of the sample. The micrographs for sample annealed at ~600 and ~1200 °C are shown in Figs. 1(c) and (d), respectively. It can clearly be seen from Figs. 1(b)–(d) that the particle size increases with annealing temperature. Such an increase has also been observed by various workers [16,17]. It is widely believed that the net decrease in free energy of solid–solid and solid–vapour interface provides the necessary driving force for particle growth during annealing process [18]. SAED of the annealed particle shown in the inset of Fig. 1(d) shows the crystallinity of larger size particles, which was later, confirmed by XRD.

3.2. X-ray diffraction

The X-ray diffractographs of as obtained and annealed samples of $Co_{0.2}Ni_{0.8}Fe_2O_4$ are shown in Fig. 2. The diffraction pattern of as obtained sample confirms the amorphous nature. On increasing the annealing temperature, the diffraction peaks become narrower and sharper, suggesting the increase in particle size and crystallinity. The particle size was calculated from most intense peak (311) using Sherrer formula [19]. It is observed that the particle size increases with the annealing temperature as shown in Fig. 3, which matches well with the TEM data. X-ray diffractographs of all the compositions ($Co_{1-x}Ni_xFe_2O_4$, where $x = 0$, 0.2, 0.4, 0.6, 0.8 and 1.0) annealed at 1200 °C are shown in Fig. 4. The lattice parameters, calculated using

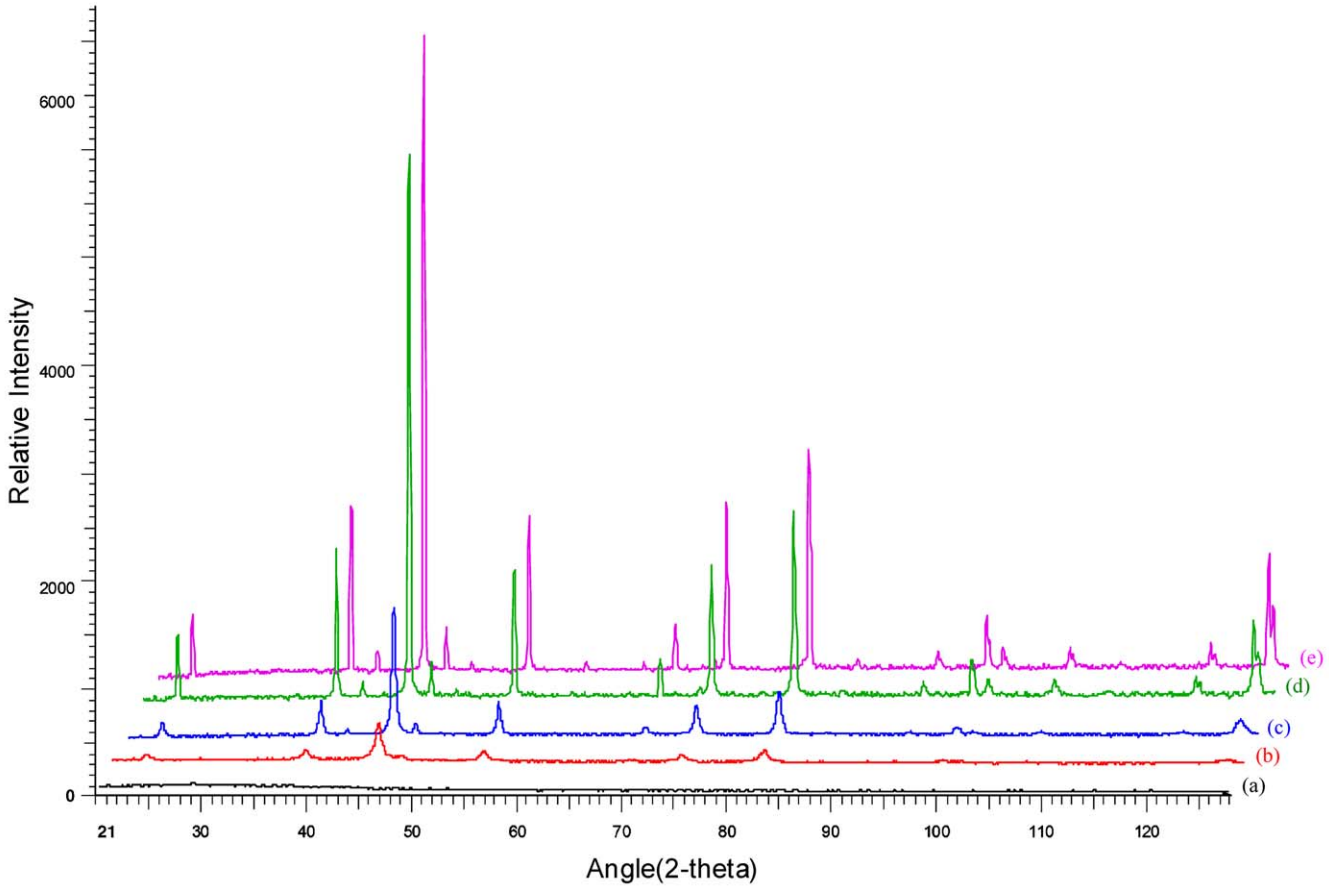

Fig. 2. X-ray diffraction pattern of $Co_{0.2}Ni_{0.8}Fe_2O_4$ (a) as obtained and after annealing at (b) 400 °C, (c) 600 °C, (d) 800 °C and (e) 1200 °C.

Powley as well as Le-Bail refinement methods (built in TOPAS V2.1 of BRUKER AXS), are listed in Table 1. All the samples were found to be face centred cubic (fcc) with *Fd*-3*m* space group. Lattice parameter '*a*' was found to decrease linearly with nickel concentration as shown in Fig. 5, which can be understood due to the smaller ionic radius of Ni^{2+} compared to Co^{2+}.

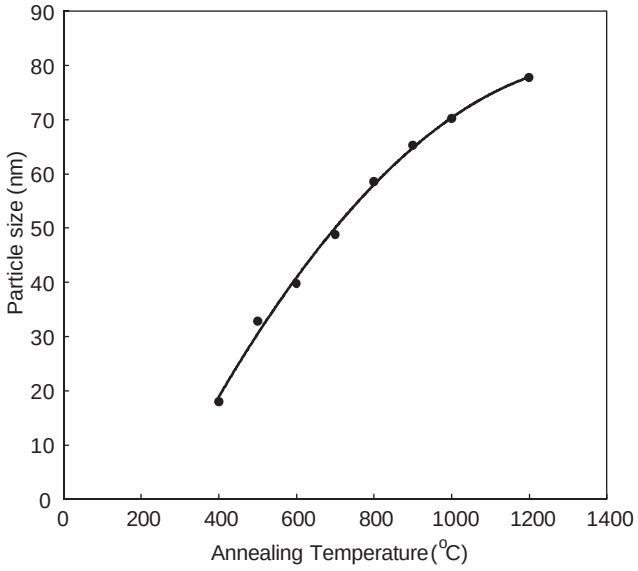

Fig. 3. Variation of particle size with annealing temperature of $CoFe_2O_4$.

X-ray density d_x was calculated using formula [20] $d_x = 8M/Na^3$ where M, N and a are the molecular weight, Avogadro's number and lattice parameter, respectively, and tabulated in Table 1. X-ray density increases linearly with nickel concentration (Fig. 5) since nickel atom is heavier that the cobalt atom.

The intensities of (220), (422) and (400) planes are sensitive to cations on tetrahedral (*A*) and octahedral (*B*) sites [21,22]. Therefore the intensities of (220), (422) and (400) plans were used to determine the cation distribution. X-ray diffraction intensity calculations were carried out using the formula suggested by Buerger [23]

$$I_{hkl} = |F_{hkl}|^2 \mathrm{PL_p},$$

where, notations have their usual meanings. It is well known [24] that, the intensity ratios $I(220)/I(400)$, $I(220)/I(440)$ and $I(400)/I(440)$ are considered to be sensitive to the cation distribution. It is known that Ni^{2+} ions have *B*-site preference, while Co^{2+} and Fe^{3+} ions can occupy both *A*- and *B*-sites [25]. Based on the above, intensity ratios for these planes were calculated

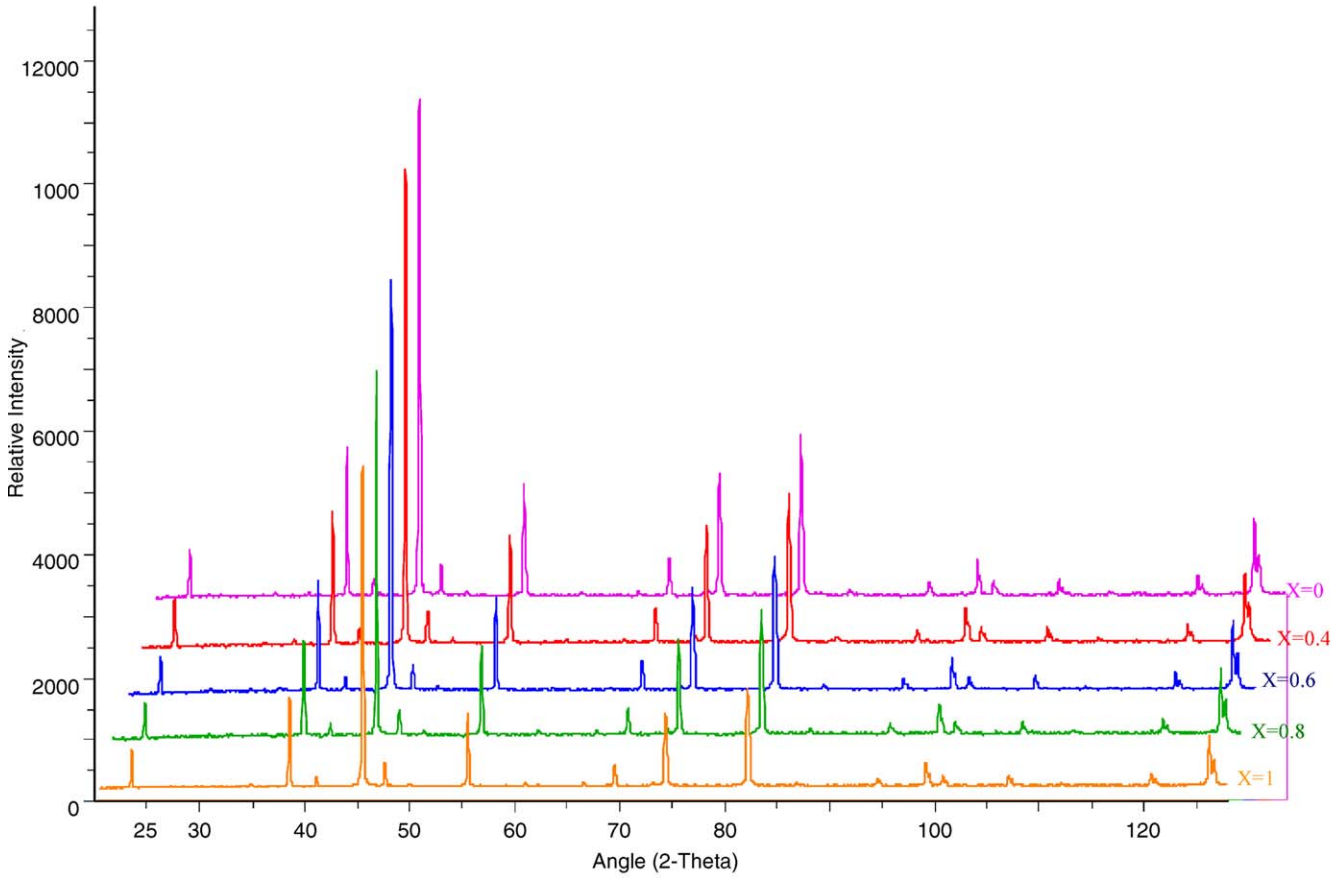

Fig. 4. X-ray diffraction pattern of $Co_{1-x}Ni_xFe_2O_4$ after annealing at 1200 °C.

for various cation distribution and those closest to experimental data are given in Table 2 for all the samples. It can be seen that the ratio of Fe^{3+}(oct.)/Fe^{3+}(tet.) decreases by replacing Ni^{2+} with Co^{2+}.

3.3. Magnetic measurements

Magnetic measurements for as-obtained and annealed samples were recorded at 300 K. Typical hysteresis loops for $CoFe_2O_4$ are shown in Fig. 6. The hysteresis loop for the as obtained sample exhibits no hysteresis, which may be attributed to superparamagnetic relaxation. The saturation magnetization of the samples annealed at 1200 °C is ~84 emu/g, which is in good agreement with the reported values [7,26]. The saturation magnetization for all the samples after annealing at 1200 °C is listed in Table 1. A decrease of saturation magnetization with the decrease in cobalt concentration can be understood by the fact that due to relatively high orbital contribution to magnetic moment Co^{2+} ions are known to give large induced anisotropy. A plot of coercivity vs. particle size (Fig. 7) shows maxima for particles of size ~35 nm which is in conformity with the other workers [27,28]. A decrease in coercivity with increase in nickel concentration may be attributed to the decrease in anisotropy field, which in turn decreases the domain wall energy [28,29].

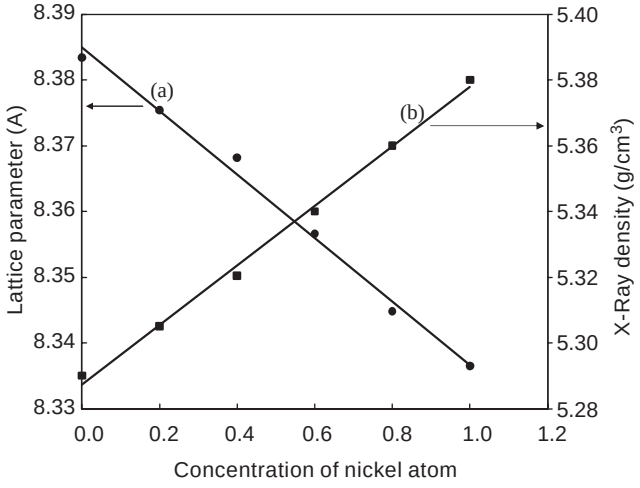

Fig. 5. Variation of (a) lattice parameter and (b) density with the nickel concentration.

3.4. Mössbauer spectroscopy

Typical Mössbauer spectra of as obtained samples of $CoFe_2O_4$ are shown in Fig. 8(a) which indicates a broad doublet due to superparamagnetic relaxation. This broad doublet was fitted with two doublets corresponding to the iron atoms residing at surface region and the internal region of the particle because for small particles, good number of atoms resides on the surface. The fitted Mössbauer data given in Table 3 indicates that the contribution of surface region atoms lie between 36% and 42%, which is in good agreement with results of Ma et al. [30]. The quadrupole splitting in the surface region (0.83–0.99 mm/s) is larger as compared to the quadrupole splitting in the internal region (0.42–0.56 mm/s) due to higher electric field asymmetry in the surface region of the particle [31]. The decrease of quadrupole splitting with the increase in Ni^{2+} concentration in this spinel structure may be due to decreased distortion in the symmetry of the electric field gradient [32].

A typical Mössbauer spectra of samples annealed at 1200 °C is shown in Fig. 8(b). The best fit could be obtained by employing two sextets attributed to tetrahedral and octahedral site [32] and data thus obtained are listed in Table 3. There is no significant change observed in the hyperfine field of all the compositions, however, the ratio Fe^{3+}(oct.)/Fe^{3+}(tet.) decreases from 2.33 to 1.04 on increasing the nickel concentration. The cation distribution was also calculated using the intensity ratio of the two sextets, also given in Table 3. The cation distribution obtained from the X-ray intensity data agrees fairly well with the cation distribution estimated from Mössbauer data.

4. Conclusions

Particle of ~10 nm size of nickel-substituted cobalt ferrites have been prepared by aerosol route. Particle

Table 2
Cation distribution data calculated from XRD pattern of the samples annealed at 1200 °C

Ferrites composition	$I_{(220)}/I_{(400)}$		$I_{(220)}/I_{(440)}$		$I_{(400)}/I_{(440)}$		Cation distribution
	Experimental	Calculated	Experimental	Calculated	Experimental	Calculated	
$CoFe_2O_4$	1.36	1.36	0.62	0.63	0.46	0.47	$[Co_{0.4}Fe_{0.6}]^A[\ Co_{0.6}Fe_{1.4}]^BO_4$
$Co_{0.8}Ni_{0.2}Fe_2O_4$	1.34	1.33	0.61	0.63	0.45	0.47	$[Co_{0.4}Fe_{0.6}]^A[Co_{0.4}Ni_{0.2}Fe_{1.4}]^BO_4$
$Co_{0.6}Ni_{0.4}Fe_2O_4$	1.3	1.31	0.61	0.62	0.52	0.47	$[Co_{0.3}Fe_{0.7}]^A[Co_{0.3}Ni_{0.4}Fe_{1.3}]^BO_4$
$Co_{0.4}Ni_{0.6}Fe_2O_4$	1.26	1.28	0.58	0.61	0.49	0.48	$[Co_{0.2}Fe_{0.8}]^A[Co_{0.2}Ni_{0.6}Fe_{1.2}]^BO_4$
$Co_{0.2}Ni_{0.8}Fe_2O_4$	1.22	1.23	0.59	0.6	0.46	0.49	$[Co_{0.2}Fe_{0.8}]^A[Ni_{0.8}Fe_{1.2}]^BO_4$
$NiFe_2O_4$	1.21	1.22	0.61	0.6	0.48	0.49	$[Fe_{1.0}]^A[\ Ni_{1.0}Fe_{1.0}]^BO_4$

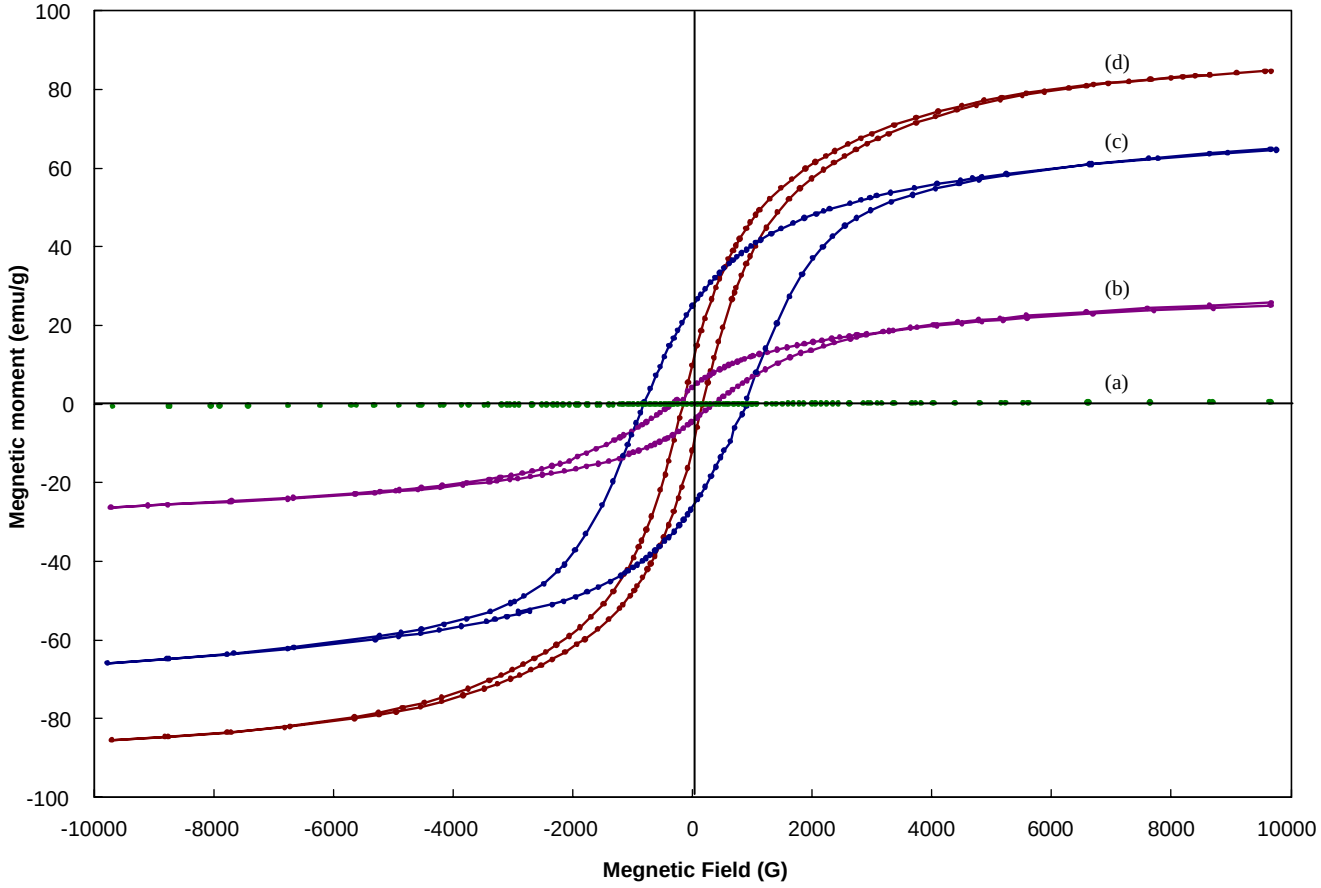

Fig. 6. Hysteresis loops for the $CoFe_2O_4$ (a) as obtained and after annealing at (b) 400, (c) 600 and (d) 1200 °C.

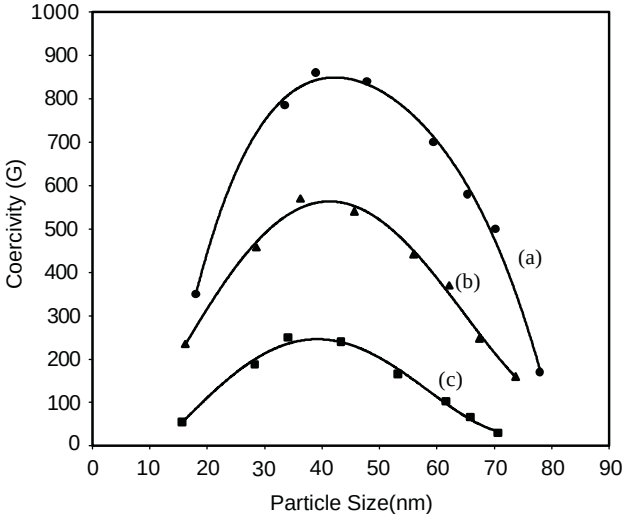

Fig. 7. Variation of coercivity with particle size for (a) $CoFe_2O_4$, (b) $Co_{0.4}Ni_{0.6}Fe_2O_4$ and (c) $NiFe_2O_4$.

size and saturation magnetization increases with the increase of annealing temperature. Mössbauer spectra suggest that, as obtained samples are superparamagnetic in nature. However, sample annealed at 1200 °C have distributed local environment of Fe-cation. The cation

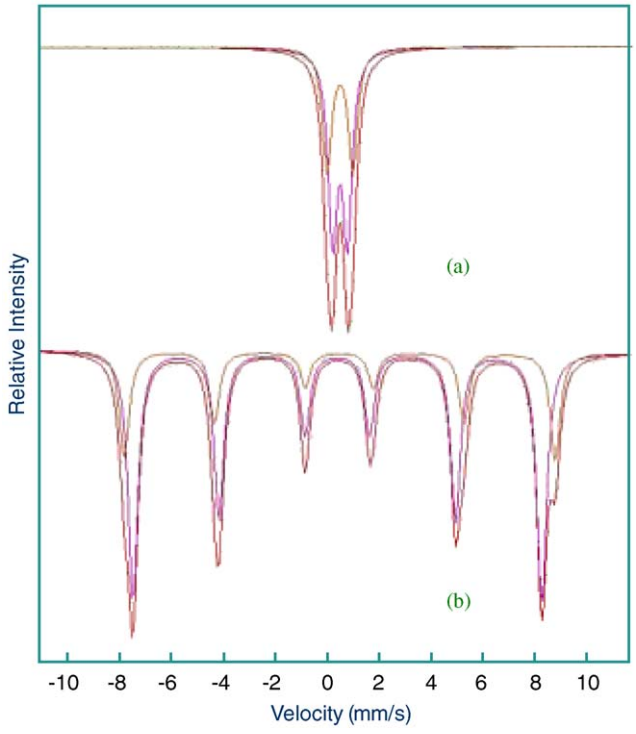

Fig. 8. Mössbauer spectra of $CoFe_2O_4$ (a) as obtained and (b) after annealing at 1200 °C.

Table 3
Mössbauer parameters of as obtained and annealed samples

Ferrites composition	As obtained					Annealed at 1200 °C					Cation distribution
	Internal region		Surface region		Surface region (%)	Tetrahedral		Octahedral		Fe^{3+}(oct.)/ Fe^{3+}(tet.)	
	δ (Fe) (mms^{-1})	ΔE_Q (mms^{-1})	δ (Fe) (mms^{-1})	ΔE_Q (mms^{-1})		δ(Fe) (mms^{-1})	H_{eff} (kOe)	δ (Fe) (mms^{-1})	H_{eff} (kOe)		
$CoFe_2O_4$	0.46	0.56	0.45	0.99	41.7	0.48	516	0.4	490	2.33	$[Co_{0.40}Fe_{0.60}]^A[Co_{0.60}Fe_{1.40}]^BO_4$
$Co_{0.8}Ni_{0.2}Fe_2O_4$	0.44	0.53	0.44	0.95	38.6	0.46	518	0.37	487	2.12	$[Co_{0.36}Fe_{0.64}]^A[Co_{0.44}Ni_{0.2}Fe_{1.36}]^BO_4$
$Co_{0.6}Ni_{0.4}Fe_2O_4$	0.46	0.49	0.45	0.92	37.5	0.49	522	0.39	493	1.94	$[Co_{0.32}Fe_{0.68}]^A[Co_{0.28}Ni_{0.4}Fe_{1.32}]^BO_4$
$Co_{0.4}Ni_{0.6}Fe_2O_4$	0.46	0.46	0.46	0.89	36.3	0.49	519	0.38	489	1.63	$[Co_{0.24}Fe_{0.76}]^A[Co_{0.16}Ni_{0.6}Fe_{1.24}]^BO_4$
$Co_{0.2}Ni_{0.8}Fe_2O_4$	0.44	0.45	0.44	0.86	40.5	0.46	524	0.36	491	1.38	$[Co_{0.16}Fe_{0.84}]^A[Co_{0.04}Ni_{0.8}Fe_{1.16}]^BO_4$
$NiFe_2O_4$	0.45	0.42	0.43	0.83	38.2	0.47	525	0.37	491	1.04	$[Fe_{1.0}]^A[Ni_{1.0}Fe_{1.0}]^BO_4$

distribution obtained from the X-ray intensity data matches very well with the cation distribution estimated from Mössbauer data.

Acknowledgments

Grateful thanks are due to the Department of Science and Technology, New Delhi for providing the grant under fast track proposal for young scientist to S.S.

References

[1] A.T. Ngo, M.P. Pileni, J. Phys. Chem. B 105 (2001) 53.
[2] M.H. Sousa, F.A. Tourinbo, J. Phys. Chem. B 105 (2000) 168.
[3] G. Bate, in: D.J. Craik (Ed.), L: Magnetic Oxides, Part 2, Wiley Interscience, New York, 1975 p. 703.
[4] M.P. Sharrock, IEEE Trans. Magn. 25 (1989) 4374.
[5] Ph. Tailhades, C. Villette, A. Rousset, G.U. Kulkarni, K.P. Kannan, C.N.R. Rao, M. Lenglet, J. Solid State Chem. 141 (1998) 56.
[6] Y. Ahn, E.J. Choi, S. Kim, H.N. Ok, Mater. Lett. 50 (2001) 47.
[7] N. Hanh, O.K. Quy, N.P. Thuy, L.D. Tung, L. Spinu, Physica B 327 (2003) 382.
[8] C.N. Chinnasamy, M. Senoue, B. Jeyadevan, O. Perales-Perez, K. Shinoda, K. Tohji, J. Colloid Interf. Sci. 263 (2003) 80.
[9] M.F.F. Lelis, A.O. Porto, C.M. Goncalves, J.D. Fabris, J. Magn. Magn. Mater. 278 (2004) 263.
[10] K.P. Chae, J. Lee, H.S. Kweon, Y.B. Lee, J. Magn. Magn. Mater. 283 (2004) 103.
[11] E.J. Cukauskas, L.H. Allen, H.S. Newman, R.L. Henry, P.K. Van Damme, J. Appl. Phys. 67 (1990) 6946.
[12] M.J. Hampden-Smith, T.T. Kodas, J. Aerosol Sci. 26 (1995) S547.
[13] Y.C. Kang, S.B. Park, J. Aerosol Sci. 26 (1995) 1131.
[14] S. Singhal, A.N. Garg, K. Chandra, J. Magn. Magn. Mater. 285 (2005) 193.
[15] T. Gonzalez-Carreno, M.P. Morales, C.J. Serna, Mater. Lett. 43 (2000) 97.
[16] J.E. Burke, Trans. Metall. Soc. AIME 180 (1949) pp. 73.
[17] J.E. Burke, D. Tunbull, Prog. Metal Phys. 3 (1952) 220.
[18] A.C.F. Costa, E. Tortella, M.R. Morelli, E.F. Neto, R.H.G.A. Kiminami, Mater. Res. 7 (2004) 523.
[19] H.P. Klug, L.E. Alexander, X-ray Diffraction Procedures for Poly Crystalline and Amorphous Materials, second ed, Wiley Interscience, New York, 1974 (Chapter 9).
[20] B.D. Cullity, Elements of X-ray Diffraction, Addition Wesley, Reading, MA, 1959.
[21] E. Eloska, W. Wolski, Phys. Stat. Solidi (A) 132 (1992) K51.
[22] B.P. Ladgaonkar, A.S. Vaingankar, Mater. Chem. Phys. 56 (1998) 280.
[23] M.G. Buerger, Crystal Structure Analysis, Wiley Interscience, New York, 1960.
[24] H. Ohnishi, T. Teranishi, J. Phys. Soc. Japan 6 (1969) 36.
[25] J.B. Good enough, A.L. Loeb, Phys. Rev. 98 (1953) 391.
[26] Y. Shi, J. Ding, H. Yin, J. Alloy Compd. 308 (2000) 290.
[27] B.S. Chauhan, J. Magn. Magn Mater. 283 (2004) 71.
[28] F. Kools, B. Hanket, Proc. ICF-5 1 (1989) 417.
[29] Y.M. Yakovlev, E.V. Rubalikaya, N. Lapovok, Sov. Phys. Sol. State 10 (1969) 2301.
[30] Y.G. Ma, M.Z. Jin, M.L. Liu, G. Chen, Y. sui, Y. Tian, G.J. Zhang, Y.Q. Jia, Mater. Chem. Phys. 65 (2000) 79.
[31] J.Y. Ying, G.H. Wang, H. Fuchs, R. Laschinsk, H. Gleiter, Mater. Lett. 15 (1992) 180.
[32] J.A. Dumesic, H. Topsoe, Adv. Catal. 27 (1977) 121.